

AD-A229 273

Parametric Studies of Multiple Fragment Interactions With Plate Array Targets

by
S. A. Finnegan
and
M. D. Alexander
Research Department

JUNE 1990

NAVAL WEAPONS CENTER
CHINA LAKE, CA 93555-6001



DTIC
ELECTE
DEC 11 1990
S E D

Approved for public release; distribution is unlimited.

90 12 11 051

Naval Weapons Center

FOREWORD

This report documents results from an experimental program involving the impact of gun-launched multiple fragments (i.e., a fragment beam) on plate array targets. Experiments were designed to study changes in target damage caused by different degrees of fragment interaction and by differences in the internal configuration of the target.

This effort was funded by the Office of Naval Research with independent research funds for the High Velocity Penetrator Effectiveness Task.

Approved by
R. L. DERR, *Head*
Research Department
11 June 1990

Under authority of
D. W. COOK
Capt., U.S. Navy
Commander

Released for publication by
W. B. PORTER
Technical Director

NWC Technical Publication 6675

Published by.....Technical Information Department
Collation.....Cover, 19 leaves
First printing.....125 copies

REPORT DOCUMENTATION PAGE

Form Approved
OMB No. 0704-0188

Public reporting burden for this collection of information is estimated to average 1 hour per response, including the time for reviewing instructions, searching existing data sources, gathering and maintaining the data needed, and completing and reviewing the collection of information. Send comments regarding this burden estimate or any other aspect of this collection of information, including suggestions for reducing this burden, to Washington Headquarters Services, Directorate for Information Operations and Reports, 1215 Jefferson Davis Highway, Suite 1204, Arlington, VA 22202-4302, and to the Office of Management and Budget, Paperwork Reduction Project (0704-0188), Washington, DC 20503.

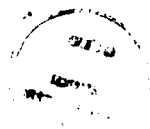
1. AGENCY USE ONLY (Leave blank)		2. REPORT DATE June 1990		3. REPORT TYPE AND DATES COVERED Summary; 1979-1980	
4. TITLE AND SUBTITLE Parametric Studies of Multiple Fragment Interactions With Plate Array Targets				5. FUNDING NUMBERS	
6. AUTHOR(S) S. A. Finnegan and M. D. Alexander					
7. PERFORMING ORGANIZATION NAME(S) AND ADDRESS(ES) Naval Weapons Center China Lake, CA 93555-6001				8. PERFORMING ORGANIZATION REPORT NUMBER NWC TP 6675	
9. SPONSORING/MONITORING AGENCY NAME(S) AND ADDRESS(ES)				10. SPONSORING/MONITORING AGENCY REPORT NUMBER	
11. SUPPLEMENTARY NOTES					
12a. DISTRIBUTION/AVAILABILITY STATEMENT Approved for public release; distribution is unlimited.				12b. DISTRIBUTION CODE	
13. ABSTRACT (Maximum 200 words) This report documents results from an experimental program involving the impact of gun-launched multiple fragments (i.e., a fragment beam) on plate array targets. Experiments were designed to study changes in target damage caused by different degrees of fragment interaction and by differences in the internal configuration of the target. Results show that the transition from Mode 1 (blast-like) to Mode 2 (penetration) damage is a gradual process. Within the transition region, methods used to identify the damage mode (e.g., the kind of damage experienced by interior target elements, the degree of fragmentation, and debris cloud momentum trends) are unreliable. For the test configurations studied, impacts below 1.8 kilometers per second (km/s) resulted only in Mode 2 damage, while impacts above 2.2 km/s resulted in Mode 1 damage provided that the distance between impacting fragments was sufficiently small.					
14. SUBJECT TERMS Blast like damage Penetration damage Fragment beam Plate array target				15. NUMBER OF PAGES 36	
				16. PRICE CODE	
17. SECURITY CLASSIFICATION OF REPORT UNCLASSIFIED	18. SECURITY CLASSIFICATION OF THIS PAGE UNCLASSIFIED	19. SECURITY CLASSIFICATION OF ABSTRACT UNCLASSIFIED	20. LIMITATION OF ABSTRACT SAR		

UNCLASSIFIED

SECURITY CLASSIFICATION OF THIS PAGE (When Data Entered)

CONTENTS

Abstract.....	3
Introduction	3
Impact Parameter Variational Experiments.....	7
Target Parameter Variational Experiments	8
Experimental Procedures	8
Data Reduction Process.....	9
Results	10
Impact Parameter Variational Experiments	10
Summary	17
Target Parameter Variational Experiments.....	17
Intermediate Impact Velocity (1.7 km/s).....	18
Summary	25
High Impact Velocity (2.2 km/s)	25
Summary	29
Fragment Beam Breakup Comparison	30
Summary	31
References.....	36



Accession For	
NTIS GRA&I	A
DTIC TAB	
Unannounced	
Justification	
By	
Distribution/	
Availability Codes	
Available and/or	
Dist	Special
A-1	

ABSTRACT

This report documents results from an experimental program involving the impact of gun-launched multiple fragments (i.e., a fragment beam) on plate array targets. Experiments were designed to study changes in target damage caused by different degrees of fragment interaction and by differences in the internal configuration of the target.

Results show that the transition from Mode 1 (blast-like) to Mode 2 (penetration) damage is a gradual process. Within the transition region, methods used to identify the damage mode (e.g., the kind of damage experienced by interior target elements, the degree of fragmentation, and debris cloud momentum trends) are unreliable. For the test configurations studied, impacts below 1.8 kilometers per second (km/s) resulted only in Mode 2 damage, while impacts above 2.2 km/s resulted in Mode 1 damage provided that the distance between impacting fragments was sufficiently small.

INTRODUCTION

Making damage predictions for complex compartmented aircraft structures impacted by high-speed multiple fragments (a fragment beam) can be very difficult. Consequently, the problem has been approached in a stepwise fashion by first conducting small-scale experiments using gun-launched fragment systems against simple plate-array targets (Reference 1). The results of these laboratory tests against simplified targets enabled investigators to identify basic damage mechanisms as well as the damage modes and the extent of damage to each. This information provided a basis upon which to formulate a simple preliminary model for predicting damage to more complex structures (Reference 2).

The preliminary model uses a generalized curve of experimental values to define residual fragment beam/target debris momentum as a function of depth into the target. The derivative of this residual curve is then determined in order to identify locations where damage potential will be the greatest. This results in an expenditure curve showing where the momentum is actually transferred to the target.

Before a momentum transfer function for an unknown structure can be determined, it is necessary to estimate the maximum invasion depth (i.e., the effective depth of collective, interacting impacts) into the target. To establish a method for making this estimate, data from small-scale impacts were analyzed using dimensional analysis techniques (Reference 3). This resulted in a nondimensional impact parameter consisting of relevant fragment beam and target variables. The invasion depths were then plotted as a function of this impact parameter. These plate array data tended to group into two linear functions, depending on the primary type of damage displayed by the target elements (Figure 1).

The fragments impacting at high speeds (2.2 kilometers per second (km/s)) suffered severe breakup. These particles were joined by finely divided target material that became entrained in the fragment beam. This applied a distributed load to the target elements, which resulted in extensive blast-like rupture damage.

At lower speeds (below approximately 1.7 km/s), fragment shatter was not significant, and the amount of entrained target material was sharply reduced. These changes in the character of the residual fragment cloud were accompanied by a proportionate increase in perforation damage and a corresponding reduction in blast-like rupture damage. In Figure 1, these two major damage modes are labeled Mode 1 and Mode 2, respectively.

At high-impact speeds, fragment cloud momentum curves have an initial plateau and distinctive rounded appearance over a wide range of target and impact conditions (Figure 2). This appearance is attributed to several factors, including large initial impact-splash momentum values associated with high-speed cratering processes. Also, the large amount of finely divided target material entrained in the residual fragment cloud as well as differences in fragment breakup rates, reduces the decay rate initially and then allows a gradual "tailing off" of the profile at the terminal end.

As impact speeds are reduced, the momentum curve gradually straightens out and begins to resemble the corresponding fragment speed profile. At speeds well below the shatter threshold, the shapes of the momentum and speed profiles are virtually identical.

From the results obtained to date, it appears that there is a close correspondence between the type of damage seen in the target and the shape of the debris momentum profile. A rounded momentum curve indicates blast-like damage, while one with an ever-increasing rate of decline (especially near the terminal end) indicates a predominance of perforation damage. There also appears to be a similar correspondence between damage mode and impact velocity; i.e., lower impact velocities are associated with perforation (Mode 2) damage, while higher ones are associated with blast-like (Mode 1) effects.

TARGET THICKNESS, mm	TARGET SPACING, cm	PROJECTILE	IMPACT VELOCITY, km/s	SYMBOL
0.41	1.91	STEEL BALLS	2.2, 1.7	○ ●
0.51	3.81	STEEL BALLS	2.2, 1.7, 1.35	△ ▲ Δ
0.81	1.91	STEEL BALLS	2.2	x
0.81	3.81	STEEL BALLS	2.2, 1.7, 1.35	□ ■
0.81	3.81	ALUMINUM BALLS	2.2	++
0.81	7.62	STEEL BALLS	2.2	+
1.27	3.81	STEEL BALLS	2.2	⊕
1.27	5.72	STEEL BALLS	2.2, 1.7	▽ ▼
1.60	7.62	STEEL BALLS	2.2, 1.7	⊗ ◆

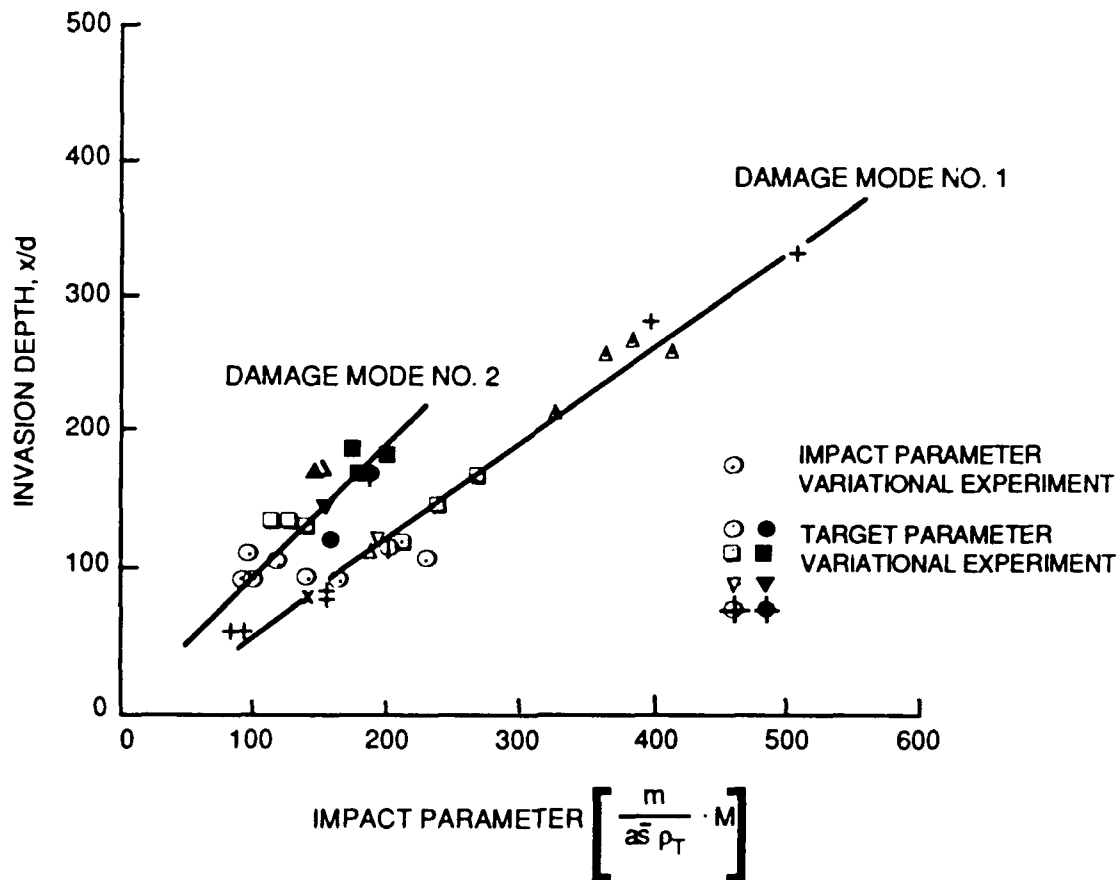


FIGURE 1. Invasion Depth Results (From Reference 2).

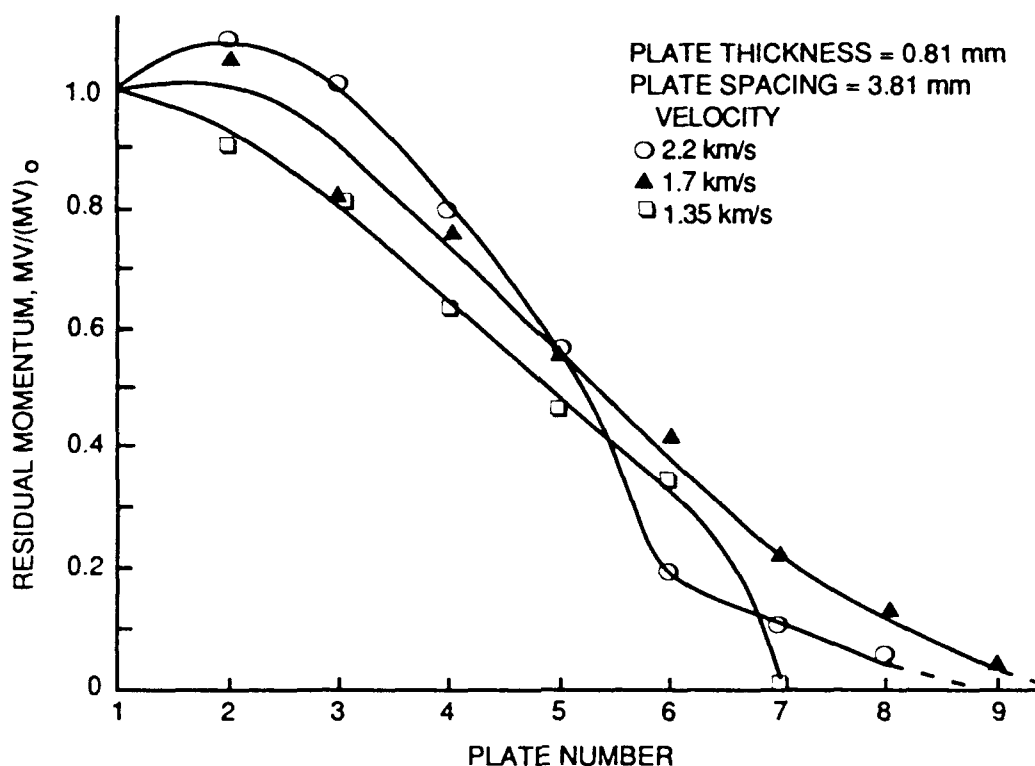


FIGURE 2. Velocity Influence on the Momentum Profile (From Reference 2).

There are impact situations, however, where these simple correspondences may not hold. One possible example would involve a high-velocity impact of a very sparsely populated fragment beam or a beam impacting over a very wide area. A second example would involve the impact of a target structure consisting of a few very thick elements rather than numerous thin ones. Both of these examples involve the possibility of changing the damage mode (i.e., from blast-like damage to penetration damage) by decreasing the degree of interaction, either initially (in the first case) or downstream (in the second case). In Figure 1, the two damage-trend lines begin to converge for small values of the impact parameter, which suggests a more "singular" form of damage in this region. A large increase in the distance between impacting fragments or in the "local" density (caused by a more heterogeneous target structure for which an averaging of density variations has less significance) would cause a shift of the impact parameter towards smaller values.

In summary, the boundaries separating these two kinds of distributed loading conditions are not well defined. In addition, the boundaries separating interactive impact conditions (involving additive or synergistic effects) from noninteractive ones are not well established. As a consequence, two sets of small-scale experiments were proposed to help define these boundaries. The results of these experiments have helped define the penetration trends shown in Figure 1. However, the rationale behind these particular tests were not discussed at that time nor were the results presented in any detail. As a result, and because of the importance of these tests in establishing fragment interaction limits, it was felt that a more extensive discussion of them was warranted. The present report summarizes these efforts.

IMPACT PARAMETER VARIATIONAL EXPERIMENTS

The first type of experiment was designed to investigate the change in damage resulting from a change in the size of the initial hit pattern. At any impact velocity, a substantial spacing between impacting fragments results in each penetrator acting independently. Additive or synergistic effects are not present to any measurable degree. Penetration damage in this case consists of individual craters or holes in the target elements.

As the hit spacing is reduced, interactive effects become significant and result in deeper penetration depths, the removal of additional target material by closely impacting fragments, and at high speeds, the blast-like rupture of interior elements of the target (Reference 1).

A series of fragment beams impacting with the same total kinetic energy, but applied over different areas, on a standard target array provides a means of studying the transition region between the two kinds of distributed loading conditions that have been observed. In addition, it provides a way to study the transition between interactive and noninteractive impacts.

TARGET PARAMETER VARIATIONAL EXPERIMENTS

The second type of experiment consisted of scaling up the size of the target structure along the impact trajectory while holding the fragment beam parameters constant. This provided a simple way of making damage comparisons on targets with the same overall average density but with internal density variations. In other words, two structures can have similar average densities with vastly different internal configurations that will respond quite differently to the same applied load. Differences in structural response should be reflected by changes in the damage mode (i.e., from rupture damage in thin elements to gross deformation, penetration damage, and translational (rigid body) motion of thicker ones), in the rate of energy absorption within the structure, and in the characteristics of the debris cloud. These factors can reflect differences in the amount, particle size, and distribution of secondary target material and in the degree of breakup and distribution of the primary fragments.

EXPERIMENTAL PROCEDURES

Fragment beams, consisting of 60 1/16-inch (1.59-mm) diameter, hard steel spheres (1 gram total mass) were launched in polycarbonate fly-apart sabots from a 50-caliber, smooth-bore powder gun. The launch velocity was measured at the muzzle of the gun using a pair of photo diodes and a time-interval counter. A thick steel plate with a center hole was positioned about 3 feet downrange from the muzzle to prevent the sabot pieces from impacting the target.

Fragment velocities at the target were measured using a six-frame, Beckman-Whitley, Kerr cell camera and a PEK Labs xenon light source. These were coupled through a 10-inch-diameter, simple condenser lens to provide shadowgraph photography.

The momentum of the residual debris cloud was measured with a ballistic pendulum coupled through a potentiometer circuit to a Hewlett Packard model 7034A x-y recorder. A heavy steel plate covered with layers of Celotex was mounted to the base of the pendulum to trap the incoming debris and impact splash.

Target elements consisted of 6-inch squares of 2024-T3 aluminum sheet material. These were weighed individually and mounted, at uniform intervals, in an open frame to allow for photographic observation. Table 1 lists the basic parameters for each experiment.

TABLE 1. Test Parameters.

Test	Target parameters			Fragment beam parameters			Impact parameters	
Impact parameter variation	Element material	Element thickness, mm	Element spacing, cm	Impactor material	Impactor diameter, mm	No. of impactors	Velocity, km/s	Hit pattern, diam., cm
	2024-T3 Al	0.41	1.90	Hard steel spheres	1.59	60	2.2	1.6-7.9
Target parameter variation	2024-T3 Al	0.41	1.90	Hard steel spheres	1.59	60	1.7	3.6
	2024-T3 Al	0.81	3.81	Hard steel spheres	1.59	60	1.7	3.5
	2024-T3 Al	1.27	5.72	Hard steel spheres	1.59	60	1.7	3.6
	2024-T3 Al	1.60	7.62	Hard steel spheres	1.59	60	1.7	3.1
	2024-T3 Al	0.41	1.90	Hard steel spheres	1.59	60	2.2	3.2
	2024-T3 Al	0.81	3.81	Hard steel spheres	1.59	60	2.2	3.0
	2024-T3 Al	1.27	5.72	Hard steel spheres	1.59	60	2.2	3.7
	2024-T3 Al	1.60	7.62	Hard steel spheres	1.59	60	2.2	3.7

DATA REDUCTION PROCESS

After each test, target elements were removed from the frame and reweighed to determine the amount of material that was removed (or, in some instances, added in the form of aluminum ablation products). Damaged areas, both impacted and ruptured, were measured and penetration depths established. The average initial spacing between impactors (i.e., initial hit spacing) was calculated using the approach described in Reference 2.

Two different penetration depths were measured. One was the distance to the furthest element impacted but not perforated by a fragment. The second was the distance over which the fragment beam acted as a unified damage agent. Evidence for collective damage was taken to be either gross rupturing or gross deformation of an element. For most of the tests, the minimum number for producing collective damage was approximately 10 fragment impacts on an element.

High-speed photographs were used to estimate the average speed along the front of the advancing debris cloud in each compartment of the target. Debris momentum values were also determined in each compartment. Repetitive testing, using a standard target and impact system, was required to obtain momentum and velocity data throughout the target structure.

RESULTS

IMPACT PARAMETER VARIATIONAL EXPERIMENTS

When these experiments were conducted, it was felt that a visual inspection of damaged target elements and simple plate measurements (e.g., mass loss measurements, dimensions of damaged regions, and penetration depths) would be sufficient for estimating the interactive penetration limits. Therefore, velocity and momentum measurements of the debris clouds were not made. A standard target array, positioned 0.6, 1.2, 1.8, 2.4, or 3.0 meters from the muzzle of the gun, was impacted at approximately 2.2 km/s with a fragment beam containing about 60 impactors (Table 1). Figure 3 shows post-impact photographs of individual plate elements from these tests, while Table 2 contains penetration measurements for each test. Normalized "collective" penetration depths ("invasion depths") are also plotted in Figure 1.

Fragment beam invasion depths for impacts with initial hit spacings larger than 0.64 centimeter (cm) cluster about the Mode 2 damage trend line in Figure 1, while those for impacts with values of 0.64 cm or less cluster about the Mode 1 line, with the exception of the data point from the test involving the smallest (0.21 cm) hit spacing. (The target structure for this particular test was very close to the gun muzzle, which resulted in a substantial loss of impactors as the outer edge of the fragment beam was also stripped off by the sabot-stopping plate. For this reason, the data point was considered to be less reliable than the others and is not shown in Figure 1, although it is still included in Table 2. Similar problems had been experienced in other tests when launching fragment beams containing large numbers (180 to 240) of impactors.)

These results indicate that a change from one damage mode (Mode 2) to another (Mode 1) can be affected by merely decreasing the average hit spacing of the impactors. The absence of any other trends in the data also suggests that there may not be any sharp distinction between Mode 2 damage and noninteractive, independent impacts.

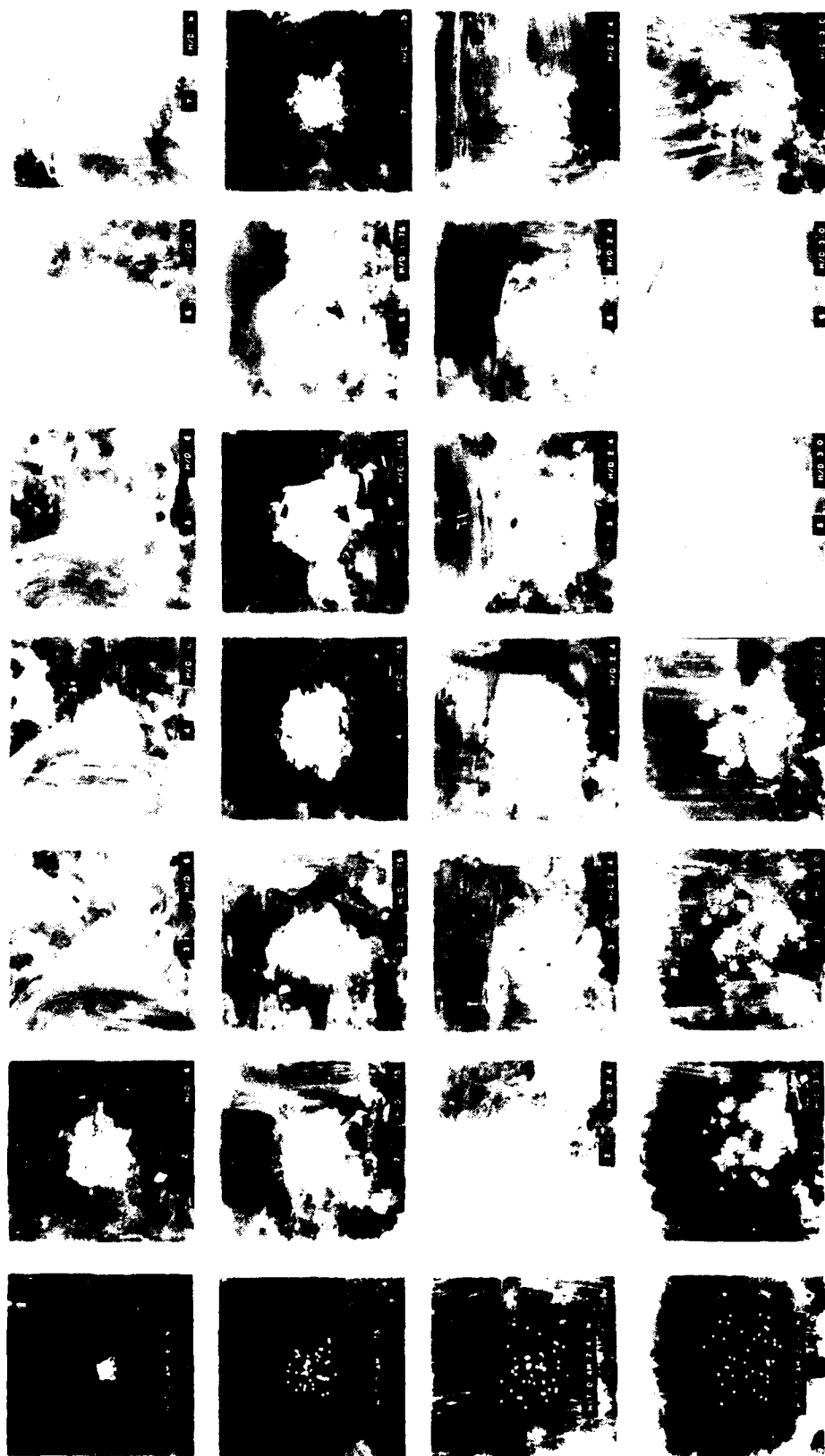


FIGURE 3. Photographs of Target Element Damage for Different Fragment Hit Spacings.

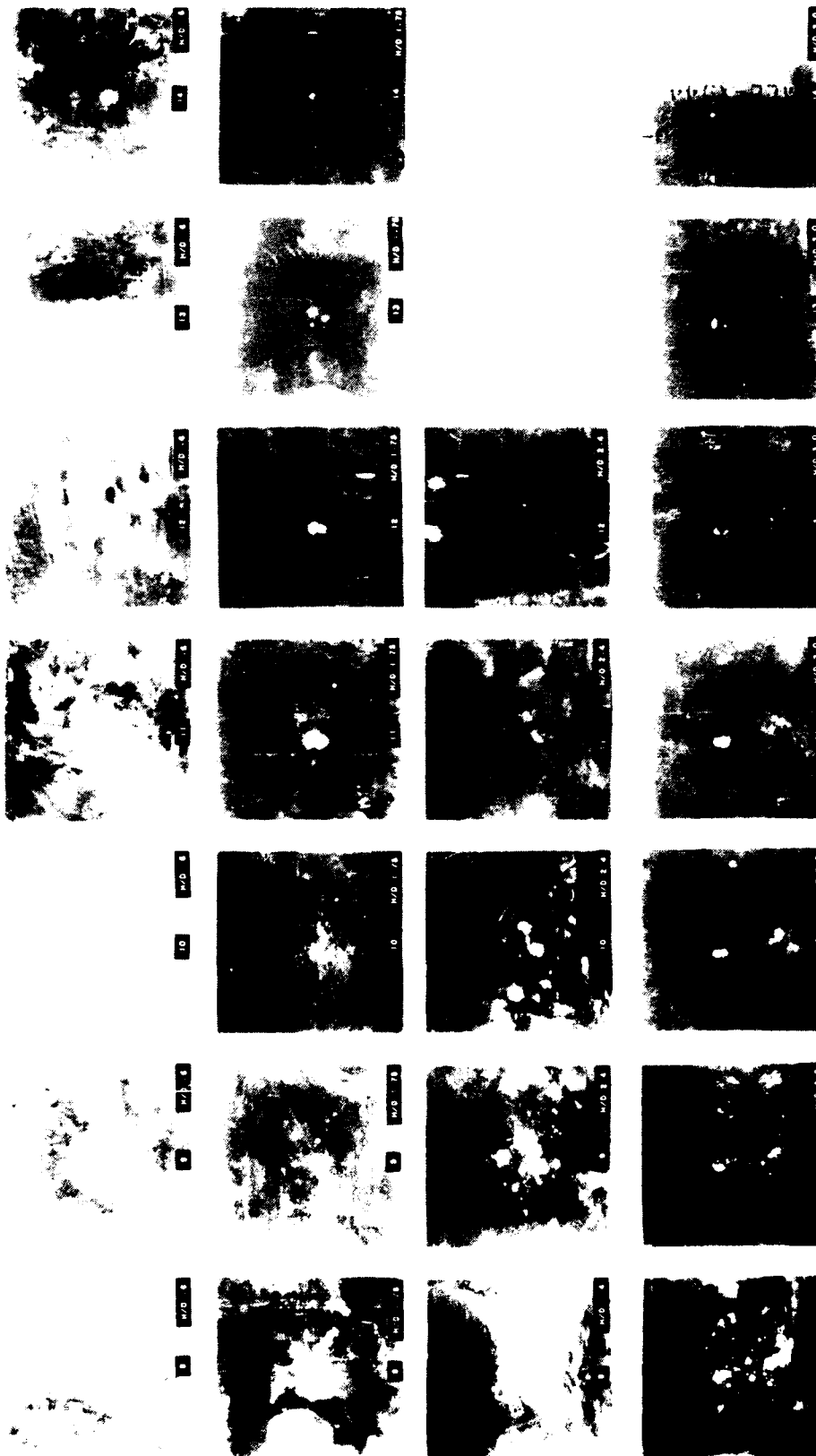


FIGURE 3. (Contd.)

TABLE 2. Penetration Data From Impact Parameter Variational Experiments.

Initial impact (hit) pattern, cm		Penetration depth, cm		
Overall diameter	Fragment spacing	Single fragment	Fragment beam ^a	Aluminum deposit
1.6	0.21	30.5	24.8	24.8
3.2	0.41	22.9	17.1	17.1
4.4	0.57	24.8	15.2	13.3
5.0	0.64	21.0	15.2	9.5
6.2	0.80	21.0	17.1	13.3
7.4	0.96	24.8	17.1	13.3
7.5	0.97	26.7	15.2	13.3
7.9	1.02	19.0	15.2	9.5

^a"Collective" invasion depth for approximately 10 impactors.

Figure 4 compares impact pattern profiles throughout the targets for different average initial hit spacings. In general, for identical target structures, an increase in the average initial hit spacing tends to increase the size of the impact patterns on the rest of the elements in the target (except for some extremely dense impact patterns that penetrate to much greater depths, as shown for the 0.21-cm hit-spacing test in Figure 4).

Within the range of hit spacings where rupture damage occurs to the target, there should be a region where an increase in the hit spacing increases the size of the ruptured area in elements close to the front of the target. (In this case, the ruptured area refers to a zone of large-scale petaling damage caused by a blast-like loading condition. Material in this zone typically peels back or tears off in large chunks.) Figure 5 compares rupture damage profiles for hit spacings of 0.21, 0.41, 0.57, and 0.80 cm. As the hit spacing is increased from 0.21 to 0.57 cm, the size of the ruptured zone increases for the third, fourth, and fifth elements of the target. For the fourth element, the size also continues to increase as the hit spacing is increased to 0.80 cm. However, the maximum rupture diameter within the target appears to remain about the same over this range of hit spacings.

If the ruptured zone is redefined to include the tear fractures around the periphery of the opening, its maximum diameter increases slightly with an increase in hit spacing from 0.21 to 0.80 cm (Figure 6). However, if the hit spacing is increased to 0.97 cm, rupture damage abruptly ceases and each impactor begins to act more independently.

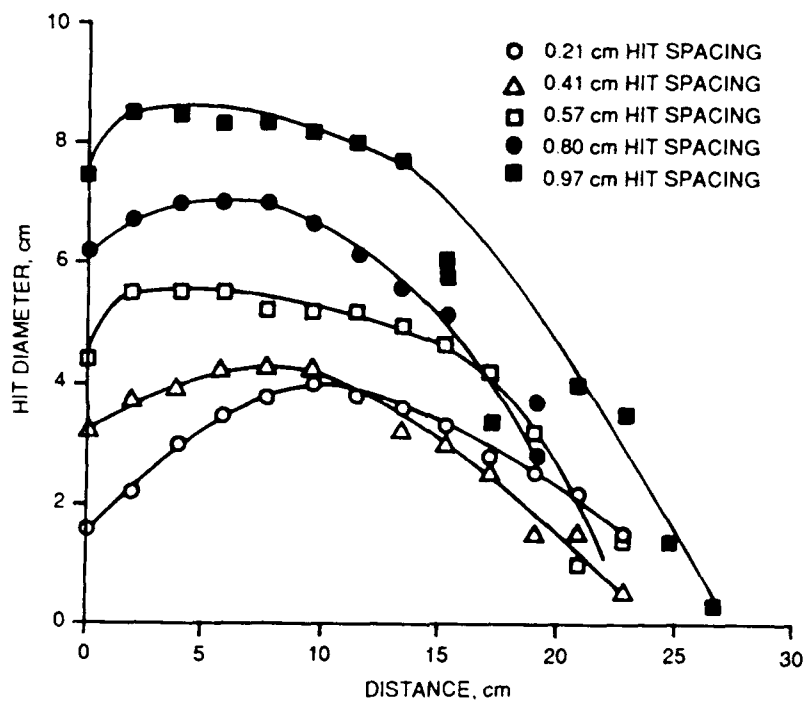


FIGURE 4. A Comparison of Impact Diameter Profiles for Different Fragment Hit Spacings.

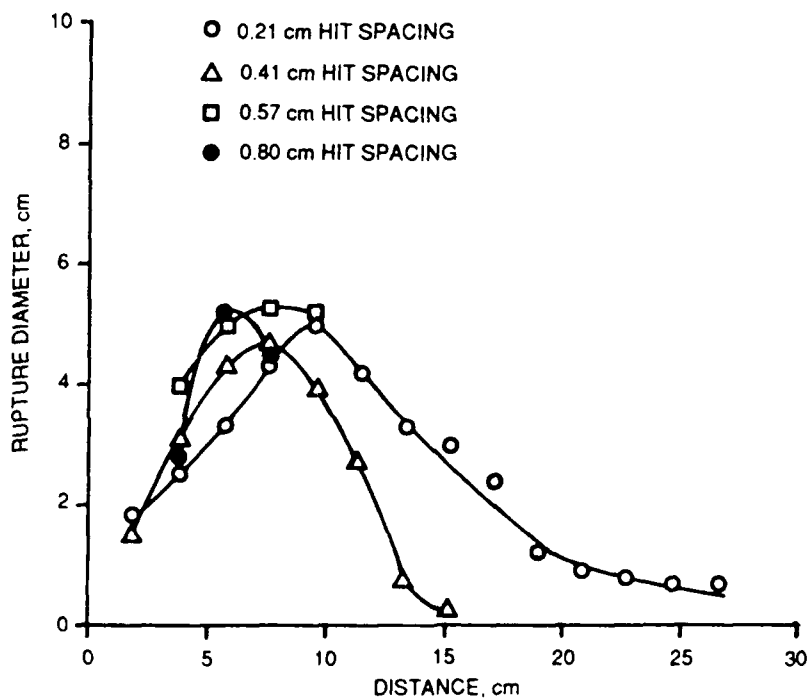


FIGURE 5. A Comparison of Rupture Diameter Profiles for Different Fragment Hit Spacings.

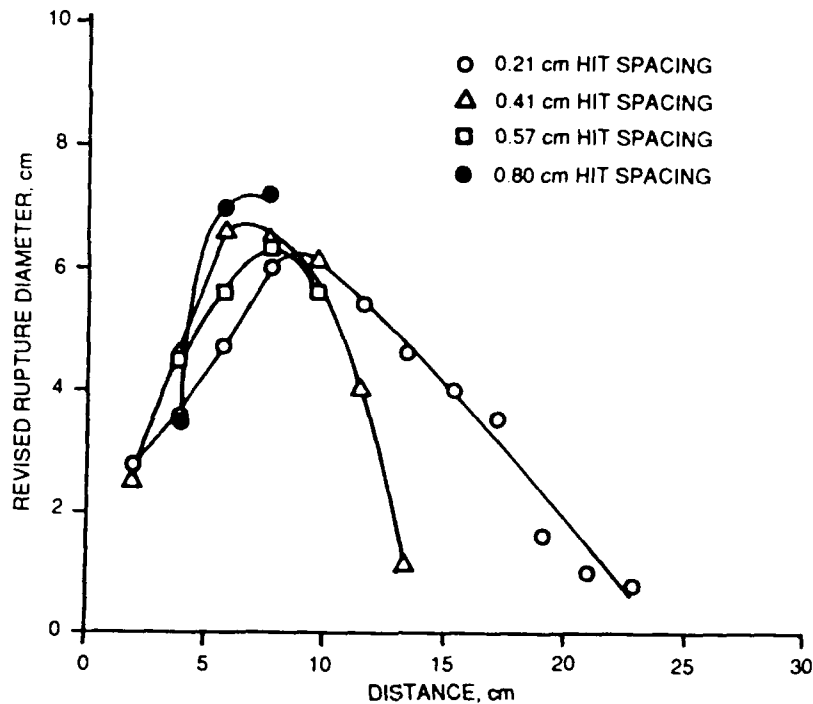


FIGURE 6. A Comparison of Revised Rupture Diameter Profiles for Different Fragment Hit Spacings.

Along with increasing the size of the ruptured zone in elements close to the front of the target, increasing the hit spacing causes the position of maximum rupture to shift one or two elements toward the front. It also results in a decrease in the number of elements that rupture (Figures 5 and 6).

The maximum mass loss for individual elements increases slightly as the hit spacing is raised from 0.21 to 0.57 cm, but then begins to drop off as the hit spacing is raised further and the amount of rupture damage diminishes (Figure 7). The total amount of material removed from each target varies inversely with hit spacing (Figure 8).

Aluminum ablation products were found on impacted elements in all of the targets tested. The furthest depth in the target that these products were found remained about the same for impacts with hit spacings of 0.57 cm or greater, but increased for impacts with smaller hit spacings (Table 2).

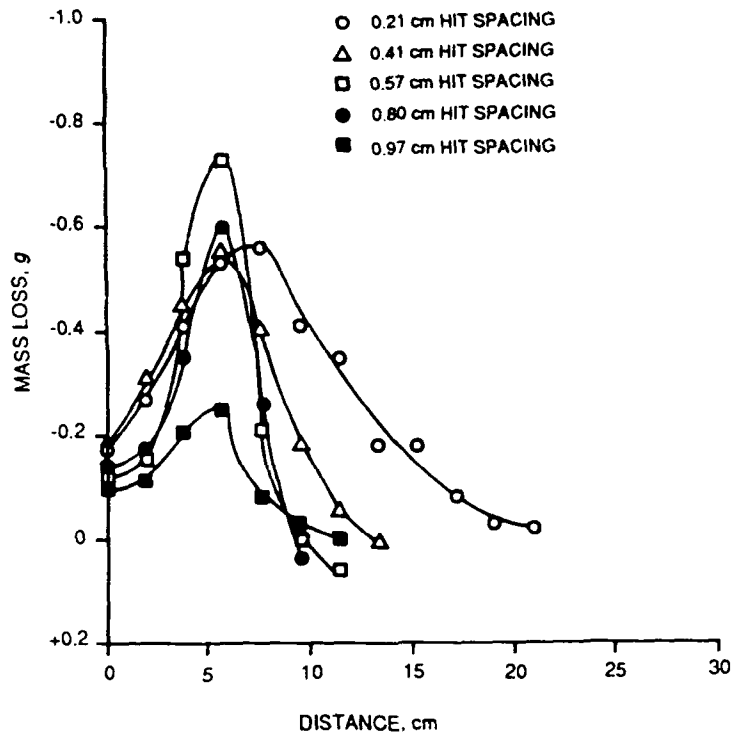


FIGURE 7. A Comparison of Target Element Mass Loss Profiles for Different Fragment Hit Spacings.

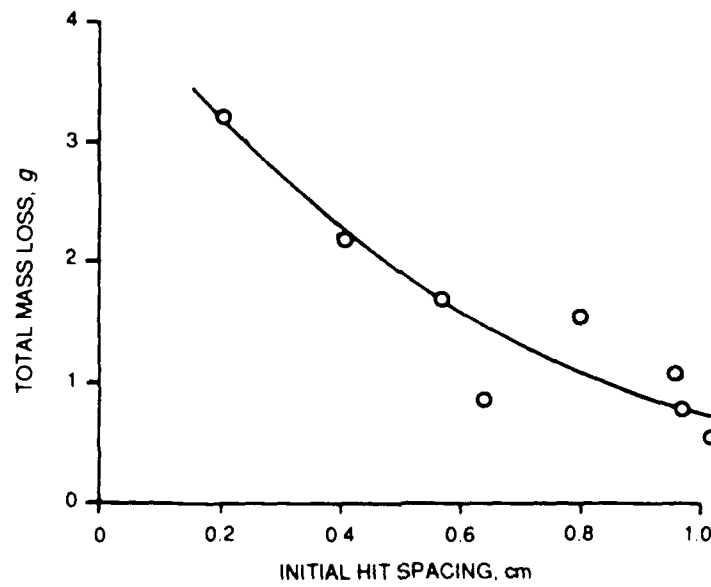


FIGURE 8. Total Target Mass Loss for Different Fragment Hit Spacings.

Summary

The major results of this particular set of experiments can be summarized as follows:

1. Impacts at 2.2 km/s with average initial hit spacings of 0.64 cm or less follow the Mode 1 damage trend line, while impacts with larger hit spacings follow the Mode 2 damage trend line. These results generally agree with the results of some recent scaling experiments involving high-speed impacts of plate array targets by multiple fragment systems (Reference 4).

2. From an inspection of the penetration data in Table 2 and damage profiles in Figures 4 through 8, it appears that the transition from Mode 1 to Mode 2 is not characterized by an abrupt change in either the amount or type of damage, but by a gradual change. For example, impacts with initial hit spacings of 0.57 and 0.80 cm show qualitatively similar damage profiles. However, the first one follows the Mode 1 damage trend line while the second follows the Mode 2 damage trend line. This observation agrees with the results described in Reference 4.

3. A visual assessment of target damage does not appear to provide conclusive evidence for a particular damage mode.

TARGET PARAMETER VARIATIONAL EXPERIMENTS

In this set of experiments, standard fragment beams containing approximately 60 impactors (Table 1) were impacted at 1.7 or 2.2 km/s against plate-array targets with the same overall density but with different plate element thicknesses (i.e., targets were scaled up in size along the flight line of the fragment beam). A single target consisted of an open frame containing 0.016-, 0.032-, 0.050-, or 0.063-inch-thick (0.4-, 0.8-, 1.3-, or 1.6-mm-thick) aluminum plates spaced 0.75, 1.5, 2.25 or 3.0 inches (1.9, 3.8, 5.7, or 7.6 cm) apart, respectively. Targets were positioned approximately 1.2 meters from the muzzle of the gun, resulting in an average initial hit spacing of about 0.44 cm at both impact velocities. High-speed photography, a ballistic pendulum, and witness plates were all used to examine the debris cloud within the target, while target element damage was assessed visually and measured as before. Figure 9 contains photographs of impacted plate elements, and Table 3 lists penetration data from the tests.

Intermediate Impact Velocity (1.7 km/s)

Figure 10 compares average speeds at the front of the debris cloud within the four target configurations impacted at 1.7 km/s. Two curves are necessary to adequately represent the data. One curve fits the data from the three targets with the thickest (0.8, 1.3, and 1.6 mm) elements. However, a separate curve is required for the data from the target with the thinnest (0.4 mm) elements because of a more rapid velocity drop for the debris cloud in this situation. The reason for this larger velocity drop is not readily apparent, although an increase in the breakup rate of the primary fragments or in the amount of fracturing of target elements would increase the rate of energy transfer to the target.

Debris cloud momentum trends for the four target configurations are sufficiently different to require separate curves (Figure 11). Curves fitting the data from the two targets with the thinnest elements have the typical rounded appearance seen at the higher impact speeds, while that for the target with the thickest elements has a shape similar to the corresponding velocity profile, which is more typical of lower-speed impacts. The curve for the target configuration with 1.3-mm-thick elements contains some features of both kinds of curves.

The size of the impact patterns on elements within the target tends to increase with the thickness of the elements (Figure 12). This increase is most likely due to the increase in distance between the elements, which allows the debris cloud to expand more laterally before impact.

The shapes of the impact pattern profiles also begin to change as the element thickness is reduced. For the target with the thickest elements, the shape is a slightly rounded one. But as the element thickness is reduced, the mid portion of the curve becomes flattened; the tail end either rises slightly before its final descent or drops sharply and then rises again for a short distance before finally dropping. Differences in the degree of fragment shatter may account for some of the differences in the shapes. In other tests, impact pattern profiles changed shape as the impact velocity was increased from 1.5 to 1.8 km/s due to the onset of fragment shatter (Reference 1).

Rupture damage is a major damage mode in the two targets with the thinnest elements (Figure 13). However, it is not significant in the other two targets where individual perforations and large deformations of the elements are the major damage forms. The gross deformation of thicker target members is considered to be a result of distributed loading.



FIGURE 9. Photographs of Target Element Damage for Different Target Sizes (2.2 km/s Initial Velocity).

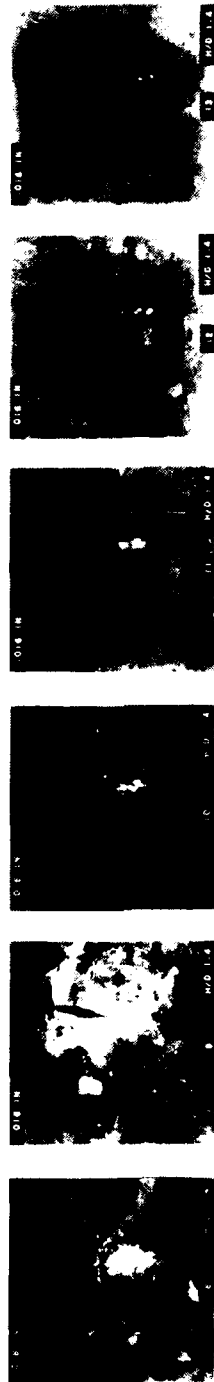


FIGURE 9. (Contd.)

TABLE 3. Penetration Data From Target Parameter Variational Experiments.

Target parameters		Impact parameters		Penetration depth, cm		
Element thickness, mm	Element spacing, cm	Velocity, km/s	Hit pattern, diam., cm	Single fragment	Fragment beam ^a	Aluminum deposit
0.41	1.90	1.7	3.6	26.7	19.0	—
0.81	3.81	1.7	3.5	34.3	30.5	—
1.27	5.72	1.7	3.6	28.6	22.9	—
1.60	7.62	1.7	3.1	30.5	22.9-30.5	—
0.41	1.90	2.2	3.2	22.9	17.1	17.1
0.81	3.81	2.2	3.0	26.7-34.3	22.9	19.0
1.27	5.72	2.2	3.7	22.9	17.1	11.4
1.60	7.62	2.2	3.7	22.9	15.2	—

^a"Collective" invasion depth for approximately 10 impactors.

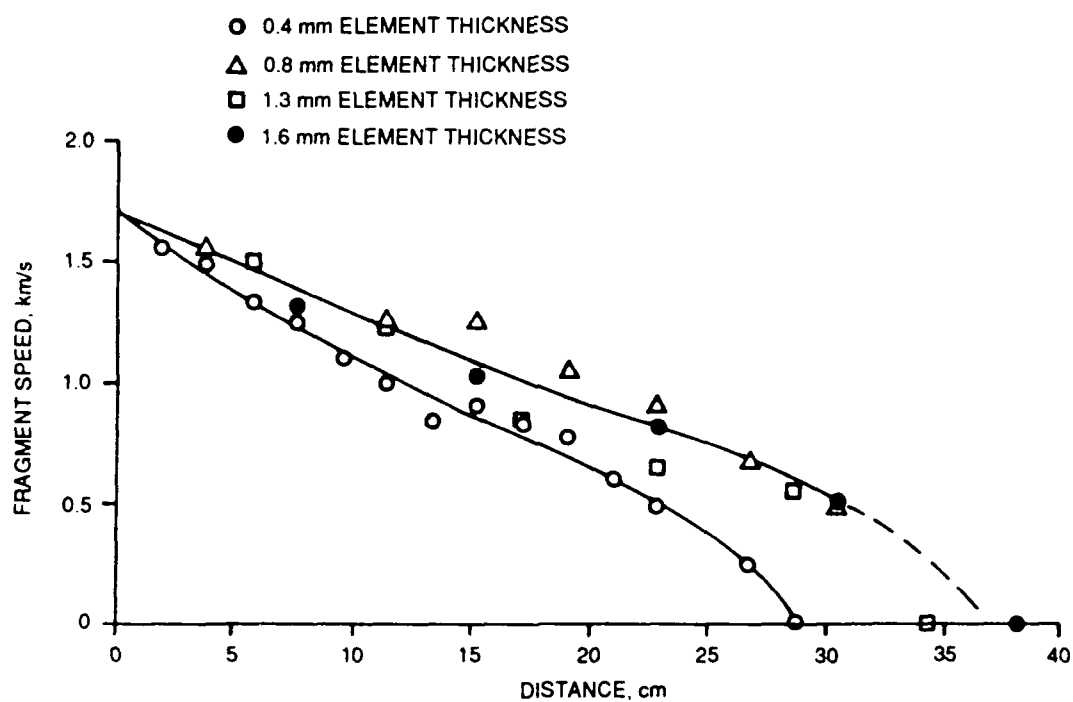


FIGURE 10. A Comparison of Debris Velocity Profiles for Different Target Sizes (1.7 km/s Initial Velocity).

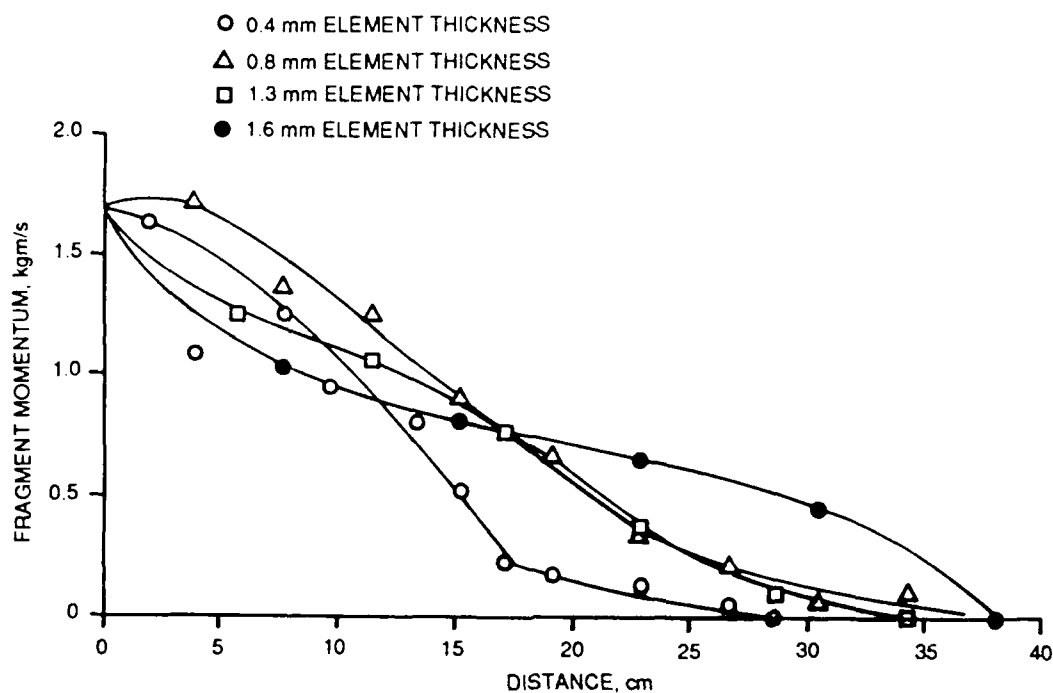


FIGURE 11. A Comparison of Debris Momentum Profiles for Different Target Sizes (1.7 km/s Initial Velocity).

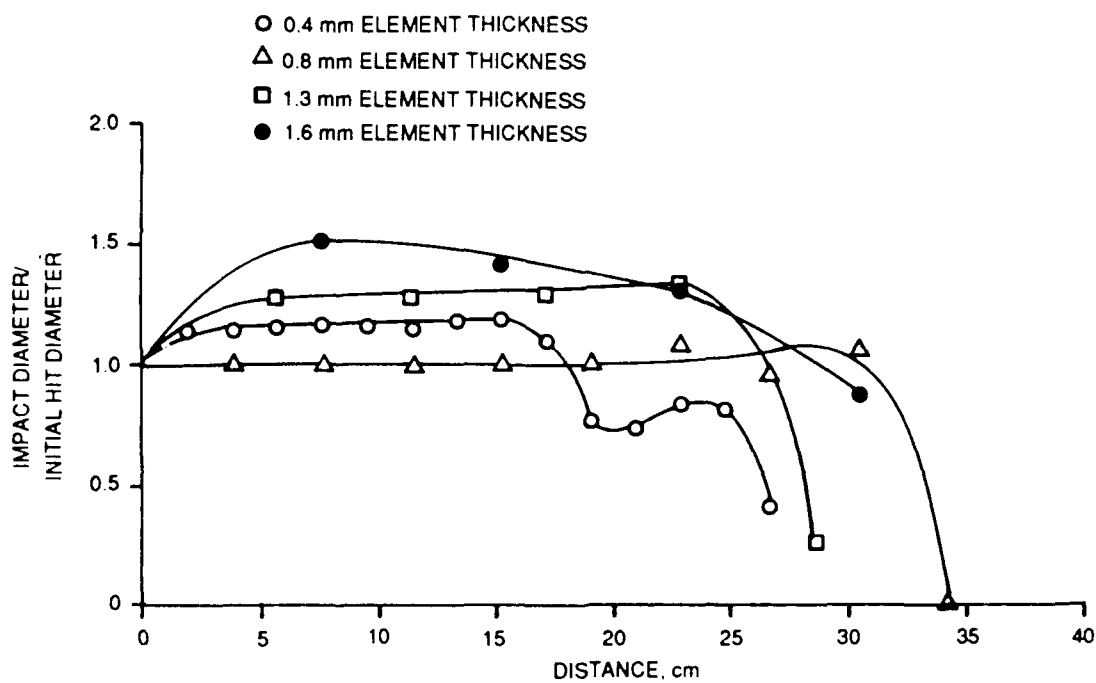


FIGURE 12. A Comparison of Normalized Impact Diameter Profiles for Different Target Sizes (1.7 km/s Initial Velocity).

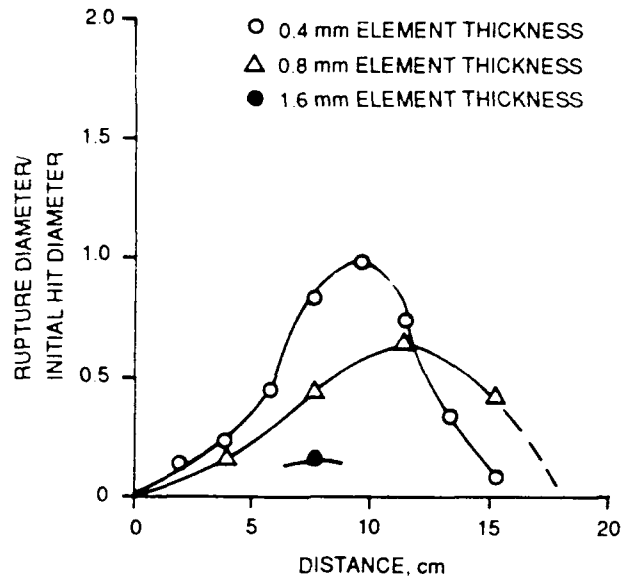


FIGURE 13. A Comparison of Normalized Rupture Diameter Profiles for Different Target Sizes (1.7 km/s Initial Velocity).

Target mass-loss profiles are shown in Figure 14. The shape of the curve reflects the primary damage mode. Targets that suffer rupture damage show a maximum loss near the center; targets that show little or no rupture damage lose the most mass on the first element, with continuously declining values seen on elements further into the target.

The total mass loss experienced by the target is shown in Figure 15. The amount of mass loss appears to be roughly proportionate to the amount of rupture damage suffered by the target.

As seen in Figure 1, invasion depths for the three targets with the thicker elements follow the Mode 2 damage trend line, while invasion depths from the target with the thinnest elements fall midway between the Mode 1 and Mode 2 damage trend lines. Whether the position of this latter point is the result of normal data scatter or a change in the damage mode was not established.

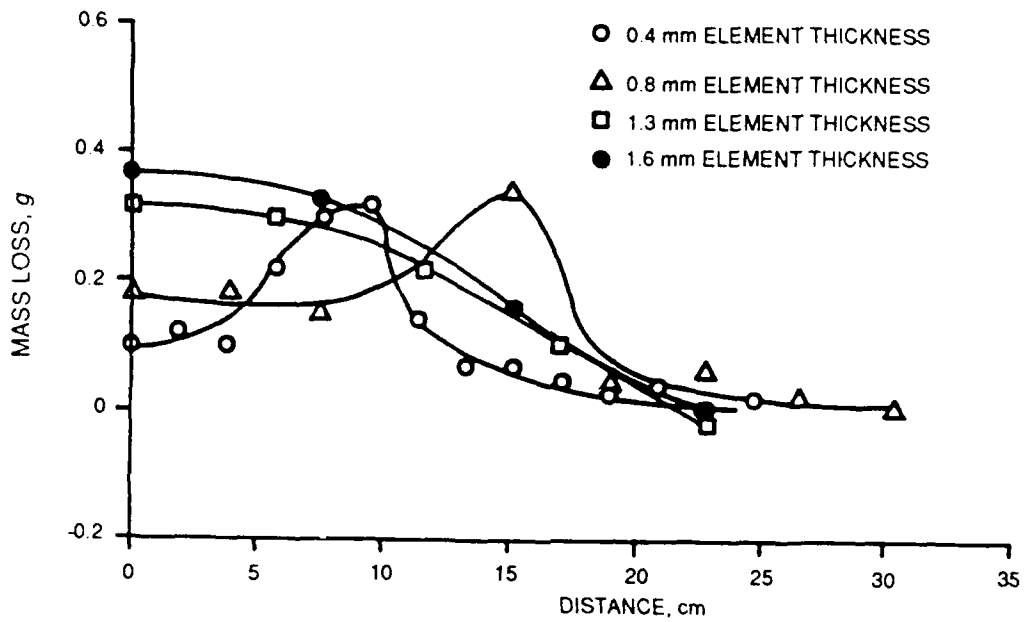


FIGURE 14. A Comparison of Mass Loss Profiles for Different Target Sizes (1.7 km/s Initial Velocity).

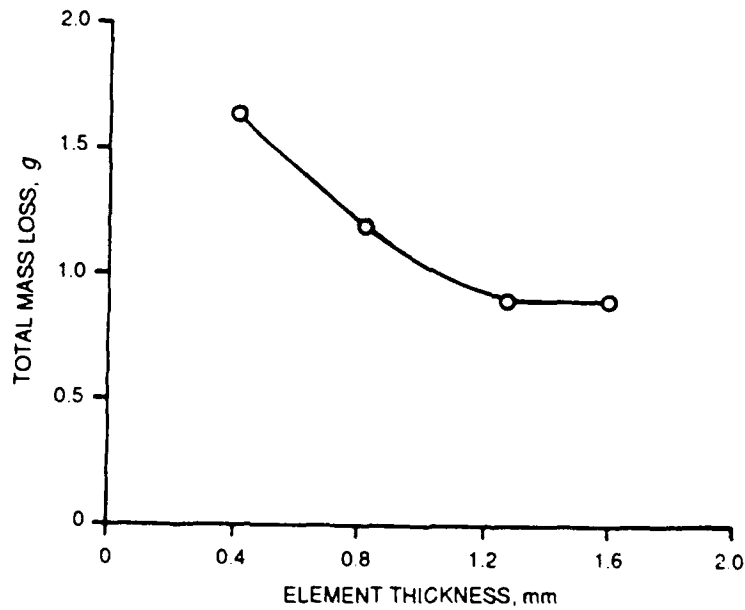


FIGURE 15. Total Mass Loss as a Function of Target Size (1.7 km/s Initial Velocity).

Summary

The primary results from impacts at 1.7 km/s can be summarized as follows:

It appears that neither the presence of blast-like rupture damage or gross deformation of target elements, or a rounded debris cloud momentum profile (all of which are characteristic of Mode 1 damage) provides conclusive evidence of this damage mode. Many of the targets that suffer Mode 2 damage (as determined by invasion depth measurements) also show these same characteristics.

High Impact Velocity (2.2 km/s)

Residual fragment debris velocities for this impact condition can be represented by a single curve (Figure 16). Although the amount of scatter is quite large if all of the data are fitted by a single curve, there are no pronounced trends, except perhaps near the terminal portions, that could be accounted for by element thickness differences as observed at the lower velocity.

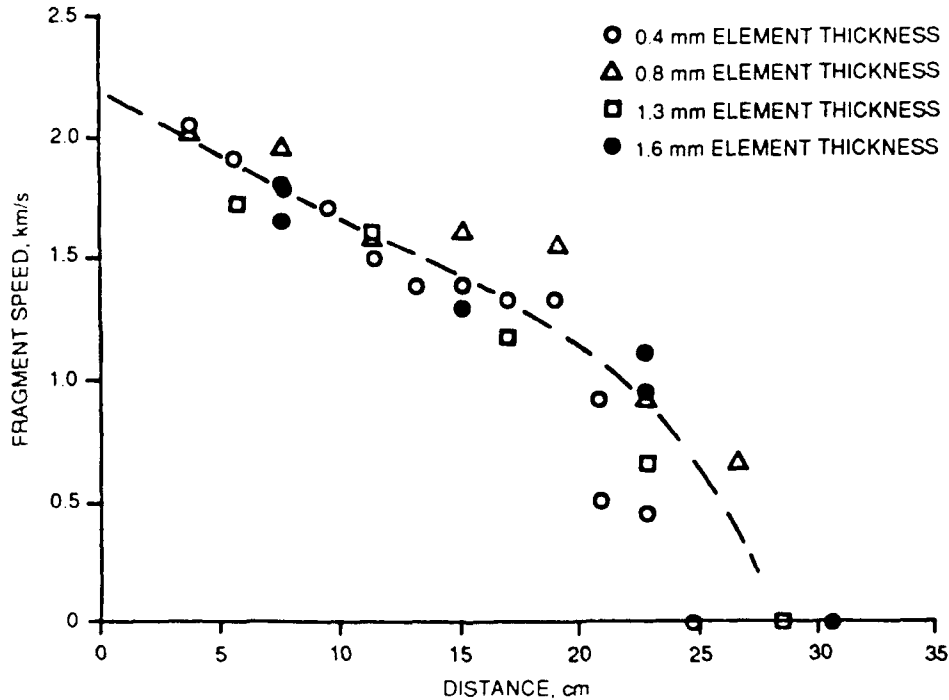


FIGURE 16. A Comparison of Debris Velocity Profiles for Different Target Sizes (2.2 km/s Initial Velocity).

The residual debris momentum data, as with the velocity data, can be fitted to a single curve (Figure 17). A rounded shape, characteristic of high-speed debris momentum trends, provides the best fit for these data. Again, the amount of scatter in the data is quite large; however, no significant correlation was found between the data and the thickness of the target elements. At first glance, a comparison of average momentum values for targets containing 0.4- and 1.6-mm-thick elements (the two thickness extremes) shows some differences near the tail end of the penetration path. However, repetitive tests at these locations resulted in such large variations in the data that the average momentum values from the two target conditions actually overlapped. At this time, the amount of data in locations where overlap occurs is probably insufficient to separate the results from the two sets of tests.

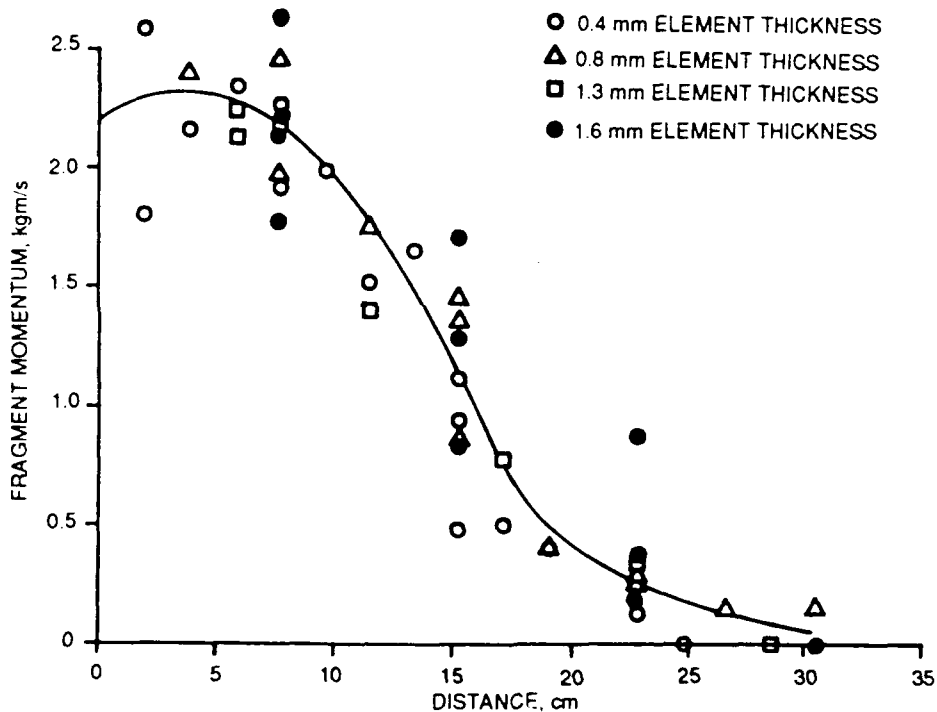


FIGURE 17. A Comparison of Debris Momentum Profiles for Different Target Sizes (2.2 Km/s Initial Velocity).

Figure 18 shows a comparison of impact diameters on the various target elements. In contrast to the variety of shapes seen at the lower impact velocity, these all have similar, smoothly rounded shapes. Those within the target increase with element thickness, in agreement with the results at the lower velocity.

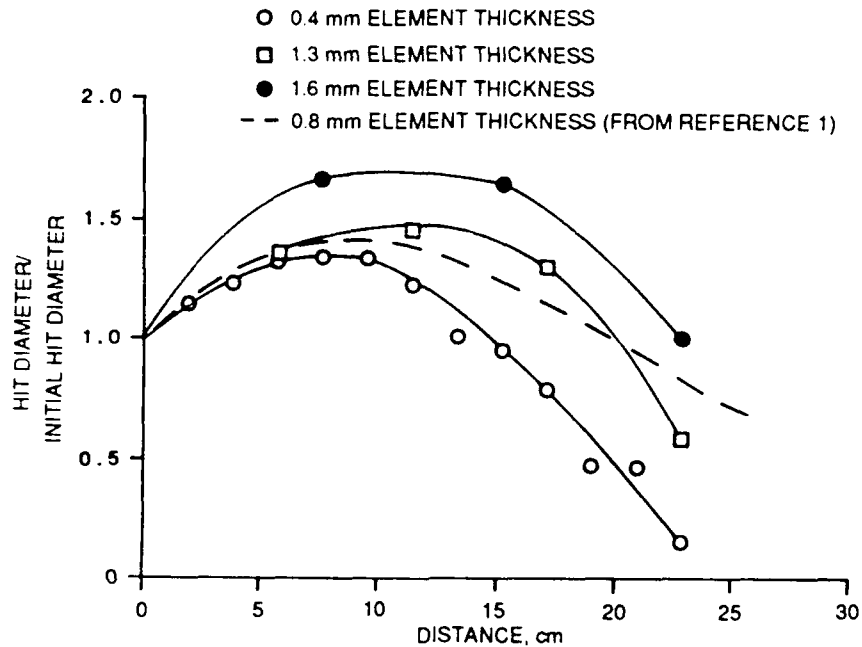


FIGURE 18. A Comparison of Normalized Impact Diameter Profiles for Different Target Sizes (2.2 Km/s Initial Velocity).

All of the targets impacted at the higher velocity show some rupture damage (Figure 19), in contrast to those impacted at the lower velocity, where only the ones containing the thinner elements ruptured. Maximum rupture occurs at roughly the same location in all of the targets.

Maximum mass loss in all of the targets occurs at approximately the same location (shown in Figure 20), which is also roughly the position for maximum rupture. Total mass loss (Figure 21) appears to increase slightly with element thickness, in contrast to the results at the lower speed where the total mass loss varied inversely with the thickness of the element.

Measured invasion depths in the targets employing 0.8-, 1.3-, and 1.6-mm-thick elements all lie essentially on the Mode 1 damage line, while the depth measured in the target with the 0.4-mm elements lies slightly to the right of this line (Figure 1). These results are consistent with the results obtained from other experiments, with similar hit spacing values, at this impact speed (References 2 and 4).

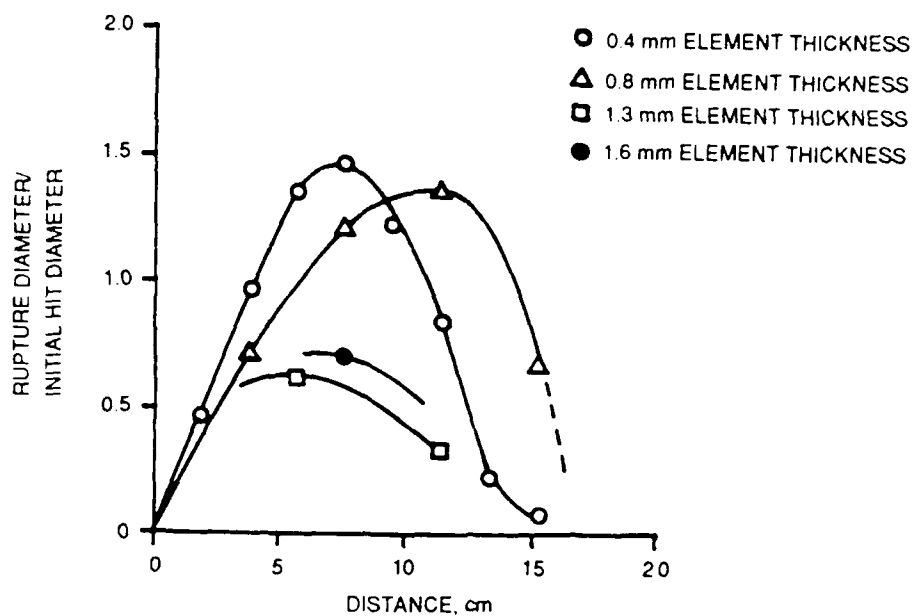


FIGURE 19. A Comparison of Normalized Rupture Diameter Profiles for Different Target Sizes (2.2 km/s Initial Velocity).

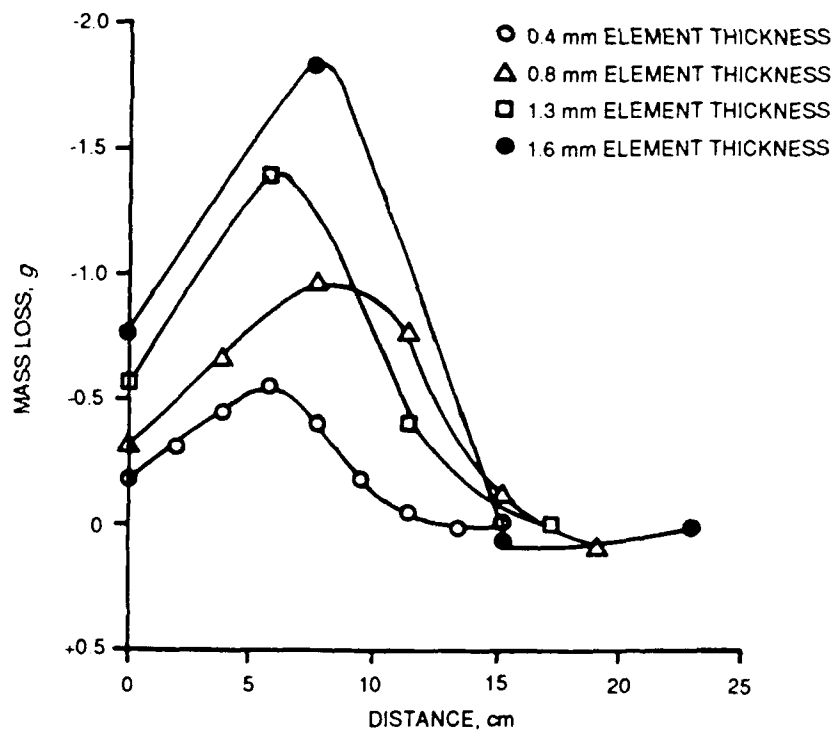


FIGURE 20. A Comparison of Mass Loss Profiles for Different Target Sizes (2.2 km/s Initial Velocity).

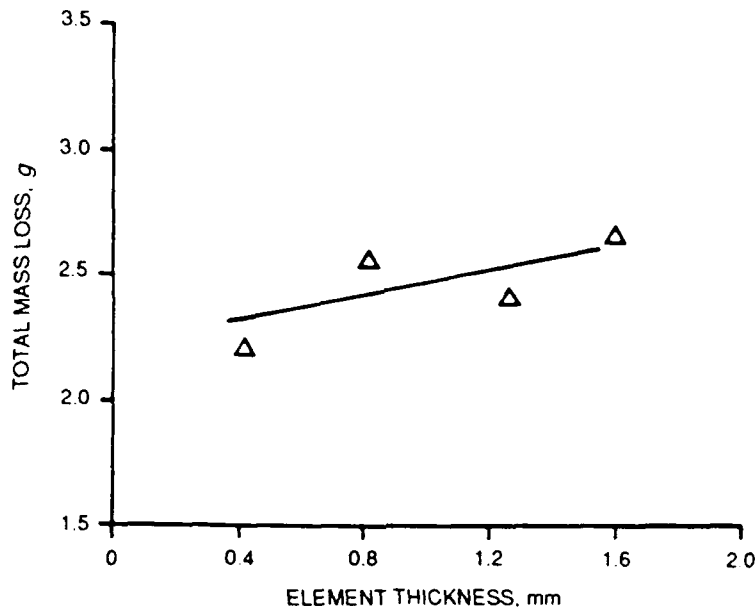


FIGURE 21. Total Mass Loss as a Function of Target Size (2.2 km/s Initial Velocity).

Summary

The important results from tests at 2.2 km/s impact speed can be summarized as follows:

1. It appears that a sufficiently high-impact speed is a requirement for Mode 1 damage. So far, all of the tests conducted at impact speeds of 1.8 km/s or less have resulted in Mode 2 damage, while those at 2.2 km/s have produced Mode 1 damage, with the exception of those with large initial hit spacing distances (Reference 4). Higher impact velocities result in an increase in the amount of target material entrained in the debris cloud, along with an increase in the degree of breakup of both the primary fragments and secondary target material. A high degree of fragment shatter and/or a large amount of finely divided target material in the debris cloud may be necessary for Mode 1 damage; this would be in agreement with the results described in Reference 4.

FRAGMENT BEAM BREAKUP COMPARISON

Size distributions from the breakup of primary fragment beam material were determined at two different locations within targets employing the thickest (1.6 mm) and thinnest (0.4 mm) elements. For the target with the thick elements, sampling took place between the first and second elements and between the second and third elements. For the target with the thin elements, sampling took place between the fourth and fifth elements and between the eighth and ninth elements. At these two locations, the fragment beam would have penetrated the same total thickness of aluminum in both targets.

For these tests, target material beyond these locations was removed and replaced with a thin, aluminum witness plate positioned 0.7 meter beyond the element being sampled. At this distance, the debris cloud was sufficiently dispersed so that impacts of individual fragments could be identified on the witness plate.

Witness plate thickness was adjusted so that the bulk of the primary fragments, initially launched at 2.2 km/s, would perforate the plate while the aluminum target fragments would embed. Initial tests used a 0.050-inch-thick witness plate. A post-impact inspection of its surface showed that too many of the primary fragments, although broken, had embedded rather than perforated.

The remainder of the tests were performed with 0.020-inch-thick witness plates. However, even with this thickness the smallest primary fragments still embedded in the witness plate. Therefore the impacts were sorted into three groups having different degrees of reliability. All perforations were considered to be the result of primary fragments and were grouped together. All embedments containing what appeared to be primary fragments were grouped in a separate category with a lower degree of reliability. The third category, with the lowest degree of reliability, contained craters with no embedded fragments. These were sorted into two additional groups depending on their shapes. The primary fragments, because of their hardness, tended to break up into irregularly shaped pieces that made similarly shaped craters in the softer, lighter aluminum. Aluminum fragments, regardless of initial shape, tended to deform and break up upon impact with the witness plate, leaving fairly smooth, broad, shallow craters with occasional streaks of metallic or oxidized aluminum around the edges.

Witness plates were divided into four segments about the center of impact and were analyzed separately. The number of segments analyzed depended on whether the hit pattern on those segments was judged to be representative of the impact pattern on the entire plate. Average hole and crater dimensions were measured using a reticle and

low-power microscope. Figures 22 through 25 display the results of these measurements.

An inspection of Figures 22 through 25 shows that the breakup rate of the primary fragments was higher in the target containing more numerous but thinner elements. Approximately 10 times as many tiny particles (below 15- to 19-mm diameter) were counted at the first sample location and about 2-1/3 times as many at the second. This result infers that the breakup rate of the primary fragments is proportional to the number of impacts suffered while traversing a given total thickness of target material.

Sintered tungsten cubes, impacting steel and aluminum plates, show a change in failure mode as the thickness of the target plate is increased (Reference 5 and data on tungsten fragment penetration gathered by S. A. Finnegan and M. E. Backman in August 1985 at NWC). Against thin targets, the cube fails, relatively undeformed by tensile processes. As the target thickness is increased, however, the cube begins to deform along the contact surface and eventually fails in this region by shear processes. Against sufficiently thick targets, the cube deforms extensively (or "mushrooms"), responding like a very ductile material.

Summary

The results of this set of experiments can be summarized as follows:

1. The breakup rate of the fragment beam increases inversely with the thickness of the target elements. It is unclear whether this increase is due to an increasing "brittleness" for impacts against very thin target members (which is probably due to the brevity of the stress wave), or to stress-wave interference effects because of the large number of collisions that the impactors experience in this situation, or to some combination of the two effects (or to other effects).

2. Because of the increase in the breakup rate, fragment beam impacts against targets composed of a multitude of thin members should result in a more rapid rate of energy transfer to the target.

NWC TP 6675

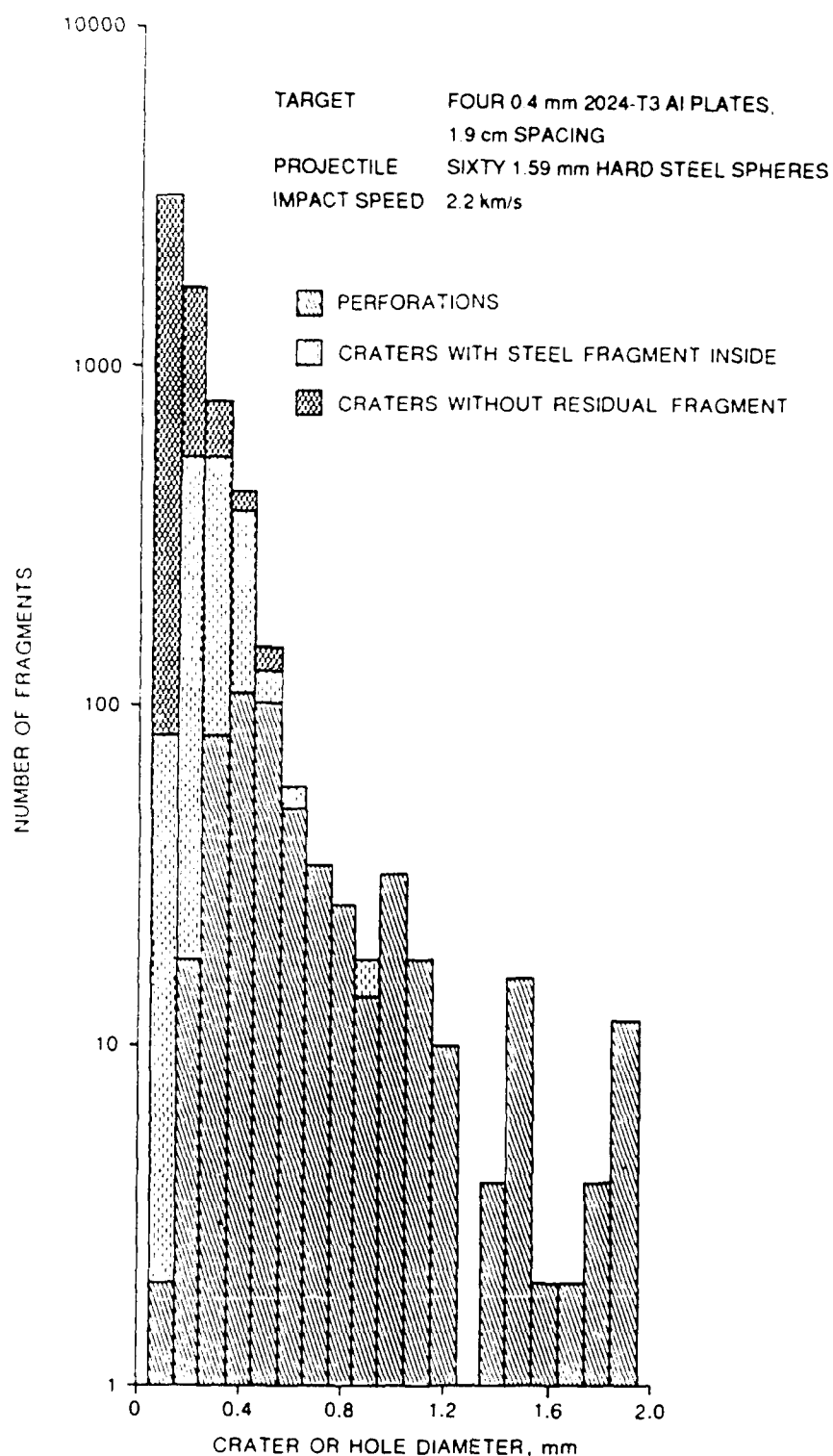


FIGURE 22. Size Distribution of Primary Fragments at the First Sample Location in the Smaller Target.

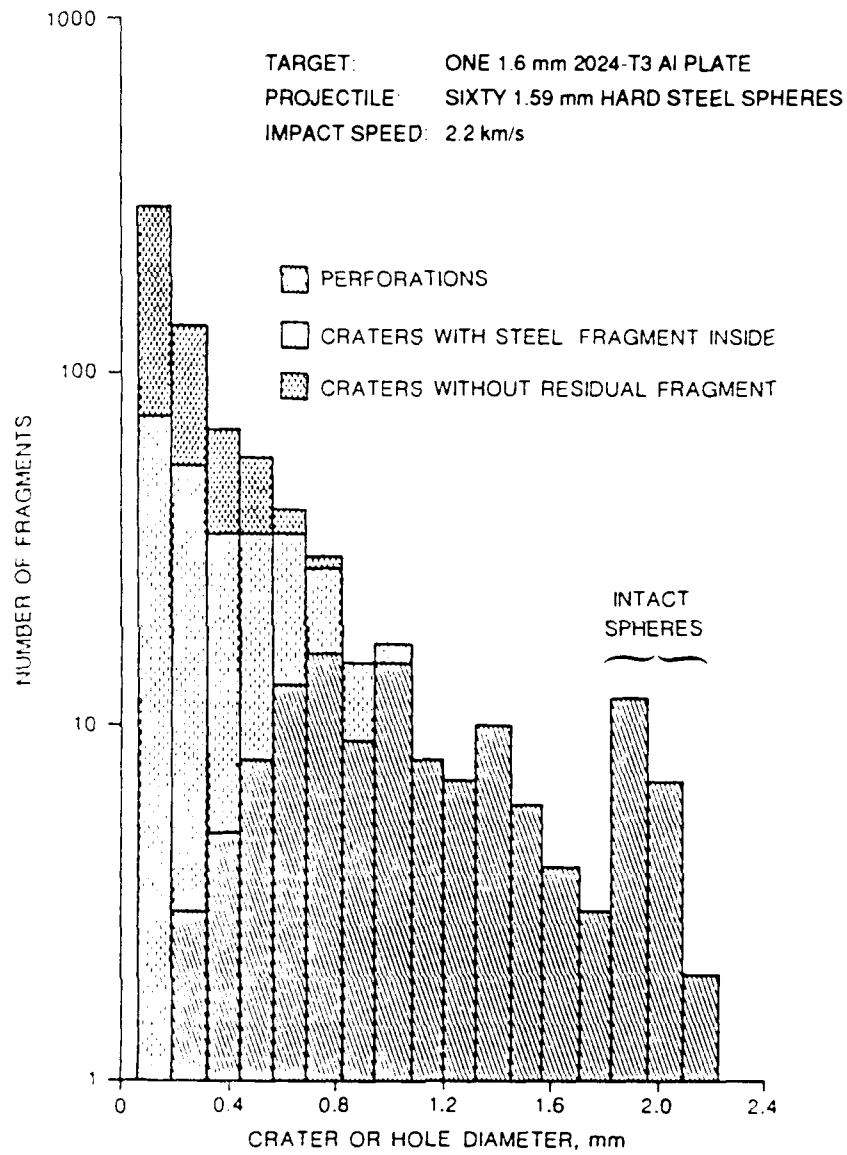


FIGURE 23. Size Distribution of Primary Fragments at the First Sample Location in the Larger Target.

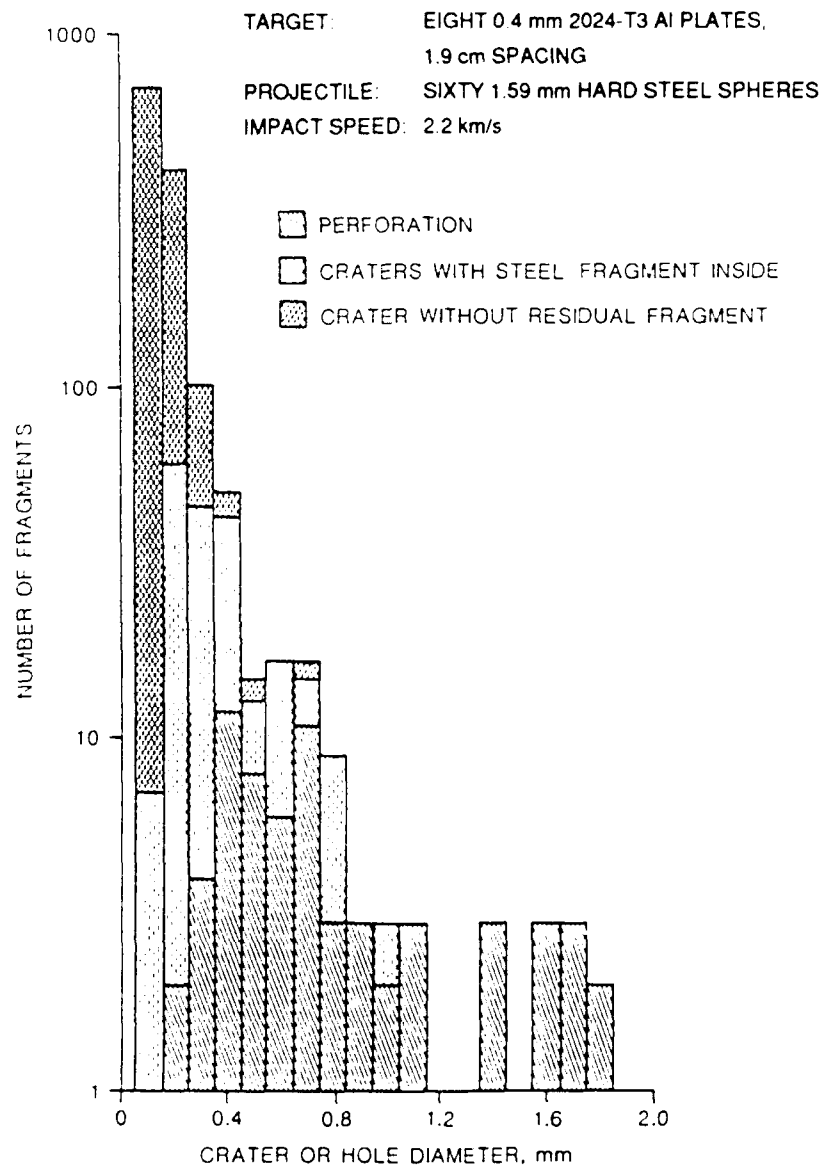


FIGURE 24. Size Distribution of Primary Fragments at the Second Sample Location in the Smaller Target.

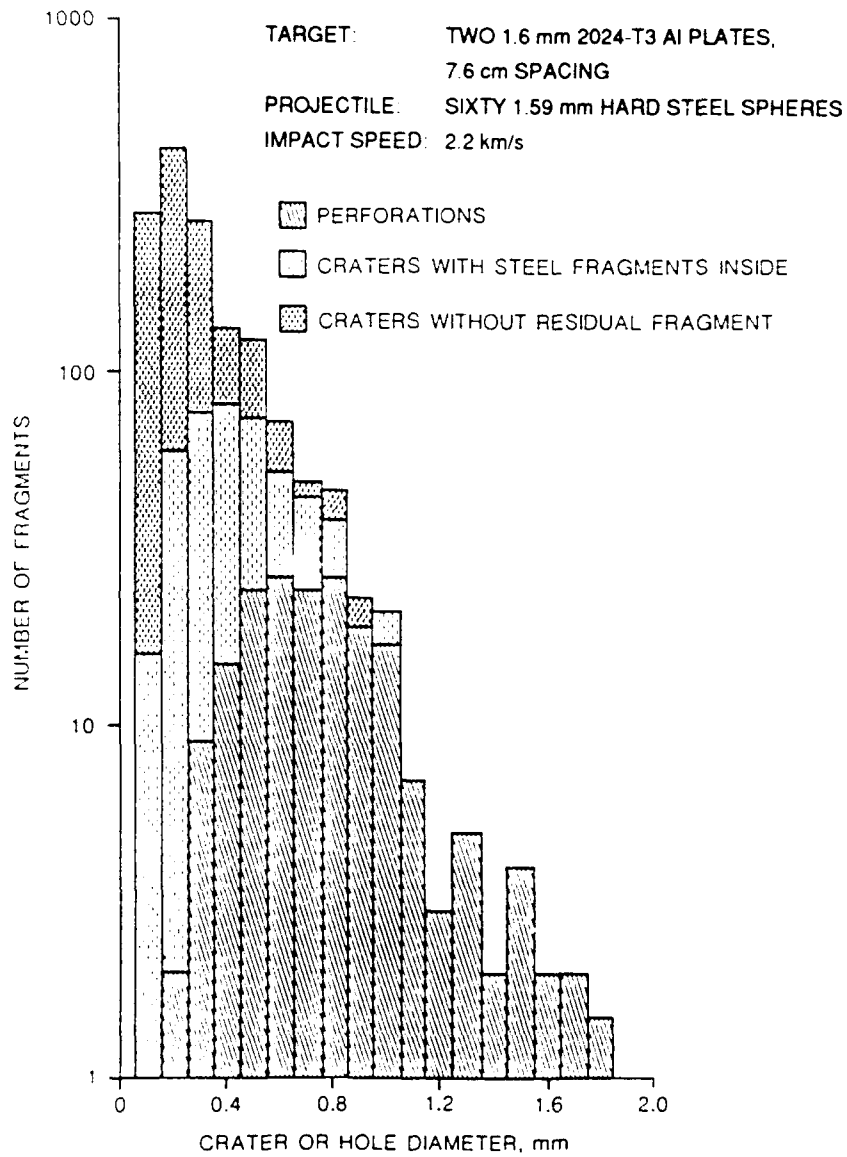


FIGURE 25. Size Distribution of Primary Fragments at the Second Sample Location in the Larger Target.

REFERENCES

1. Naval Weapons Center. *Interaction of Multiple Fragment Systems with Plate Array Targets*, by Mark D. Alexander and Stephen A. Finnegan. China Lake, Calif., NWC, January 1979. (NWC TP 6058, publication UNCLASSIFIED.)
2. Mark D. Alexander and Stephen A. Finnegan. "A Model for Multiple Fragment Interactions in 3-D Targets", in *Proceedings of the Seventh International Symposium on Ballistics, The Hague, The Netherlands*, 19-21 April 1983.
3. Wilfred E. Baker, Peter S. Westine, and Franklin T. Dodge. *Similarity Methods in Engineering Dynamics*. Rochelle Park, N.J., Hayden Book Co., 1978.
4. Mark D. Alexander, Stephen A. Finnegan, and Roberta A. Zimmerman. "A Study of Scaling Effects in the Modeling of Multiple Fragment Impacts", in *Proceedings of the Tenth International Symposium on Ballistics*, San Diego, Calif., 27-29 October 1987.
5. Naval Weapons Center. *Penetration Equations for Tungsten Fragments*, by Rodney F. Recht and Stephen A. Finnegan. China Lake, Calif., NWC, April 1987. (NWC TP 6768, publication UNCLASSIFIED.)

INITIAL DISTRIBUTION

- 11 Naval Air Systems Command
 - AIR-5004 (2)
 - AIR-5401B (1)
 - AIR-5401B1 (1)
 - AIR-5403 (2)
 - AIR-9301 (2)
 - AIR-932 (1)
 - AIR-932D (1)
 - PMA-259 (1)
- 5 Chief of Naval Operations
 - OP-03 (2)
 - OP-05 (1)
 - OP-091 (1)
 - OP-55 (1)
- 1 Space and Naval Warfare Systems Command (SPAWAR-005)
- 1 Chief of Naval Research, Arlington (OCNR-10P)
- 7 Naval Sea Systems Command
 - SEA-62D (5)
 - Technical Library (2)
- 1 Commander in Chief, U. S. Pacific Fleet, Pearl Harbor (Code 325)
- 1 Air Test and Evaluation Squadron 5, China Lake
- 1 Commander, Third Fleet, San Francisco
- 1 Commander, Seventh Fleet, San Francisco
- 1 David Taylor Research Center, Bethesda
- 2 Naval Academy, Annapolis (Director of Research)
- 1 Naval Air Force, Atlantic Fleet
- 2 Naval Air Force, Pacific Fleet
- 1 Naval Air Station, North Island, San Diego
- 2 Naval Air Test Center, Patuxent River (Central Library, Bldg. 407)
- 1 Naval Avionics Center, Indianapolis (Technical Library)
- 1 Naval Explosive Ordnance Disposal Technology Center, Indian Head (Technical Library)
- 1 Naval Ocean Systems Center, San Diego (Technical Library)
- 1 Naval Ordnance Station, Indian Head (Technical Library)
- 1 Naval Postgraduate School, Monterey (Technical Library)
- 1 Naval Surface Warfare Center, Dahlgren (Code G-13, D. Dickinson)
- 4 Naval Surface Weapons Center, White Oak Laboratory, Silver Spring
 - Guided Missile Warhead Section (1)
 - Technical Library (3)
- 1 Naval War College, Newport (Technical Library)
- 1 Office of Naval Technology, Arlington (OCNR-20)
- 1 Operational Test and Evaluation Force, Atlantic
- 1 Pacific Missile Test Center, Point Mugu (Technical Library)
- 1 Marine Corps Air Station, Beaufort
- 1 Army Materiel Systems Analysis Activity, Aberdeen Proving Ground (AMXSY-AD, C. Alston)
- 2 Army Research Office, Research Triangle Park
 - DRXPO-IP-L, Information Processing Office (1)
 - Dr. E. Saible (1)
- 1 Harry Diamond Development Center, Adelphi (Technical Library)
- 1 Redstone Arsenal (Rocket Development Laboratory, Test and Evaluation Branch)
- 2 Rock Island Arsenal
 - Navy Liaison Office (NVLNO) (1)
 - SARRI-ADM-P, Technical Library (1)

- 3 Air Force Munitions Systems Division, Eglin Air Force Base
 - AFATL/FXW (1)
 - AFATL/DLODL, Technical Library (1)
 - AFATL/SAA (1)
- 1 Air Force Intelligence Agency, Bolling Air Force Base (AFIA/INTAW)
- 1 Air University Library, Maxwell Air Force Base
- 1 Tactical Fighter Weapons Center, Nellis Air Force Base (CC/CV)
- 1 Defense Nuclear Agency (Shock Physics Directorate)
- 2 Defense Technical Information Center, Alexandria
- 1 Department of Defense - Institute for Defense Analyses Management Office (DIMO), Alexandria
- 1 Lawrence Livermore National Laboratory, University of California, Livermore, CA (Technical Library)
- 1 Lewis Research Center (NASA), Cleveland, OH
- 1 Los Alamos National Laboratory, Los Alamos, NM (Reports Library)
- 2 Applied Research Associates, Lakewood, CO
 - R. F. Recht (1)
 - J. D. Yatteau (1)
- 1 California Institute of Technology, Jet Propulsion Laboratory, Pasadena, CA (Technical Library)
- 2 Colorado Seminary, Denver Research Institute, Denver, CO
 - Applied Mechanics Laboratories (1)
 - Technical Library (1)
- 1 Hercules, Incorporated, Allegany Ballistics Laboratory, Rocket Center, WV (Hercules Aerospace Producers Group)
- 1 Hudson Institute, Incorporated, Center for Naval Analyses, Alexandria, VA (Technical Library)
- 1 IIT Research Institute, Chicago, IL (Department M, Document Librarian)
- 1 Stanford Research Institute, Poulter Laboratories, Menlo Park, CA
- 2 The Johns Hopkins University, Applied Physics Laboratory, Laurel, MD (Document Library)
- 1 The Rand Corporation, Santa Monica, CA (Technical Library)

ON CENTER DISTRIBUTION

- 1 Code 326, McCubbin
- 1 Code 3261
- 4 Code 343 (3 plus Archives Copy)
- 2 Code 3686, GIDEP
- 1 Code 37, J. Wunderlich
- 1 Code 372, T. Loftus
- 1 Code 38
- 1 Code 389
- 26 Code 3894
 - S. Finnegan (20)
 - O. E. R. Heimdahl (1)
 - A. Lindfors (1)
 - J. K. Pringle (1)
 - J. C. Schulz (1)
 - M. Wagenhals (1)
 - K. Woods (1)